Science Advances
AAAS

advances.sciencemag.org/cgi/content/full/6/25/eabb2393/DC1

Supplementary Materials for

Programmable and scalable transfer printing with high reliability and efficiency for flexible inorganic electronics

Chengjun Wang, Changhong Linghu, Shuang Nie, Chenglong Li, Qianjin Lei, Xiang Tao, Yinjia Zeng, Yipu Du, Shun Zhang, Kaixin Yu, Hao Jin, Weiqiu Chen, Jizhou Song*

*Corresponding author. Email: jzsong@zju.edu.cn

Published 17 June 2020, *Sci. Adv.* **6**, eabb2393 (2020)
DOI: 10.1126/sciadv.abb2393

The PDF file includes:

Thermal analysis of the TRT stamp under the absorbed laser power of Si ink.
Bending deformation analysis of the Si pellets on TRT stamp.
Evaluation of the relation between the applied laser power from the laser system and the absorbed laser power of Si pellet.
Figs. S1 to S18
Legends for movies S1 and S2

Other Supplementary Material for this manuscript includes the following:

(available at advances.sciencemag.org/cgi/content/full/6/25/eabb2393/DC1)

Movies S1 and S2

Thermal analysis of the TRT stamp under the absorbed laser power of Si ink

An axisymmetric finite element model is established in COMSOL Multiphysics to investigate the temperature distribution of the TRT stamp under the absorbed laser power of silicon pellet. The schematic geometry model, as illustrated in fig. S4A, consists of a block of PDMS as the temporary receiver substrate, a Si pellet as the ink and the TRT stamp. The thermal conductivity, density and heat capacity are 0.15 $Wm^{-1}K^{-1}$, 970 kg/m^3 and 1460 $Jkg^{-1}K^{-1}$ for PDMS (*24*), 150 $Wm^{-1}K^{-1}$, 2300 kg/m^3 and 708 $Jkg^{-1}K^{-1}$ for Si (*24*) and 0.16185 $Wm^{-1}K^{-1}$, 12.736 kg/m^3 and 1352 $Jkg^{-1}K^{-1}$ for the TRT stamp from experimental measurements. The ambient temperature is 25°C and convection coefficient is set as 7 $Wm^{-2}K$. The power is applied via a heat source to the upper surface of the Si ink.

Bending deformation analysis of the Si pellets on TRT stamp

A three-dimensional finite element model is established in ABAQUS to simulate the bending deformation of the Si pellet array adhered on the TRT stamp. The schematic geometry model is illustrated in fig. S4C, where the Si pellets are attached on the TRT stamp consisting of the adhesive layer and backing layer. The Young's modulus and Poisson's ratio are 130 GPa and 0.3 for the Si pellet, 21 MPa and 0.49 for the adhesive layer of the TRT stamp, and 350 MPa and 0.42 for the backing layer of the TRT stamp, respectively. The thickness is 3 μm for the Si pellet, 50 μm for the adhesion layer, and 100 μm for the backing layer of TRT, respectively. The C3D8 element is used to discretize the structures.

Evaluation of the relation between the applied laser power from the laser system and the absorbed laser power of Si pellet

During thermal analysis in FEA, we assume that the laser energy from the programmable laser system can directly transmit the PDMS receiver substrate and be absorbed completely by the Si pellet to heat the TRT stamp into weak adhesion state. Thus, the Si pellet is modeled as the heat source and the laser power is applied to the upper surface of Si pellet in FEA. In practical applications, due to the optical reflectivity and transmission loss of the Si pellet and PDMS receiver substrate, the applied laser power from the programmable laser system is required a relatively higher than the absorbed laser power of the Si pellet. Here, the relation between applied laser power P_a of the programmable laser system and the absorbed laser power P_s of the Si pellet is obtained based on a simple theoretical evaluation by following the previous work (*24*) and reads as

$$P_a\left(1-\varsigma_{\mathrm{Si}}\right)\left(1-\chi_{\mathrm{Si}}\right)\frac{\pi R^2}{a^2}=P_s, \tag{1}$$

where ς_{Si} and χ_{Si} are the reflectivity and transmission of the Si pellet, R and a are the diameter of the laser spot and in-plane size of the square Si pellet, respectively. The reflectivity and absorption

loss of the PDMS is neglected here. The transmission χ_{Si} of a 3 μm thick silicon nanomembrane under the given laser wavelength of 808 nm (coefficient of absorption, 7.75×10^2 cm^{-1}) can be calculated as 0.793. With the reflectivity 0.328 for polished silicon (*24*), diameter of the laser spot 350 μm, and in-plane size of the Si pellet 350 μm×350 μm. The required applied laser power is around 0.137 W for the absorbed laser power of the Si pellet of 15mW, which is consistent to the applied laser power during experiment, i.e. 0.15 W.

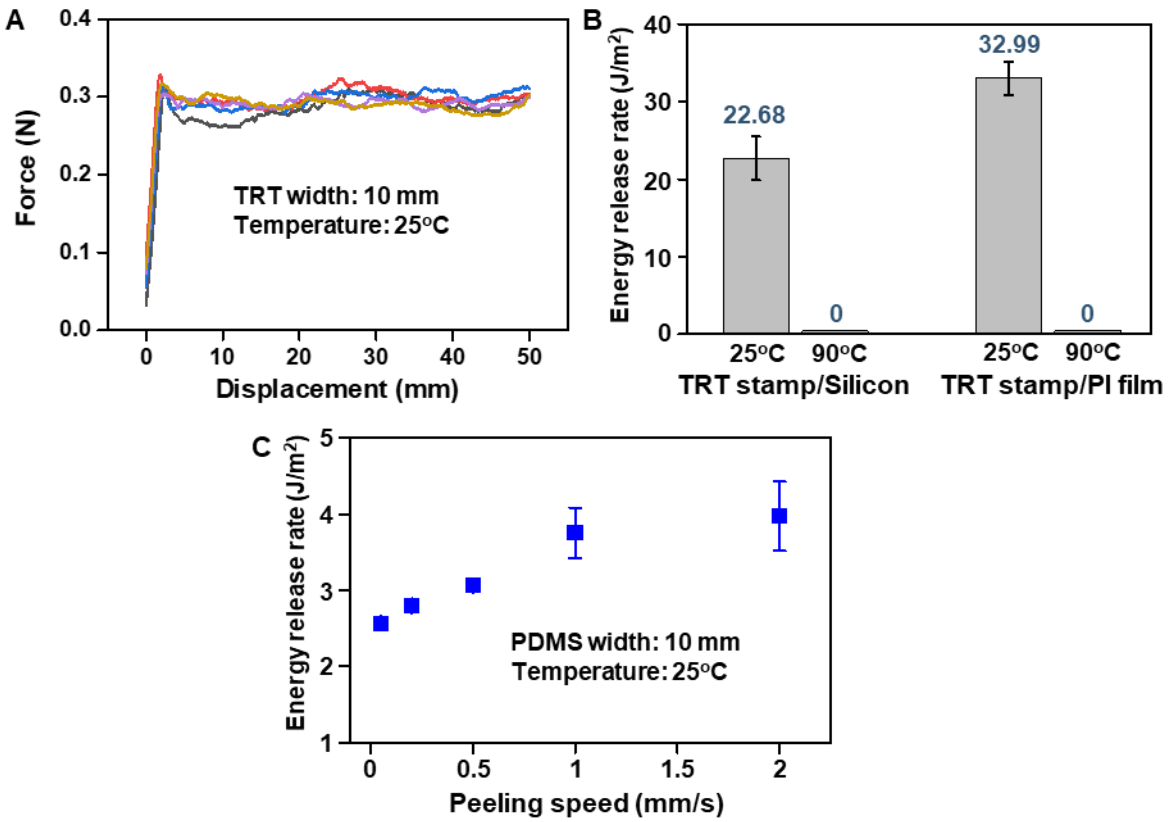

Fig. S1. The adhesion strength characterization of TRT stamp. (**A**) Force versus displacement curve of TRT stamp with glass slide during 90º peeling test at 1 mm/s constant peeling speed. (**B**) The measured energy release rate of TRT stamp with the materials used for devices fabrication, i.e. polished silicon wafer and PI film. The adhesion force of TRT stamp after heated at 90°C is too small to measure with the load cell. (**C**) The measured energy release rate of PDMS slab (1 cm×10 cm) of 1 mm thickness with polished silicon wafer at various peeling speed.

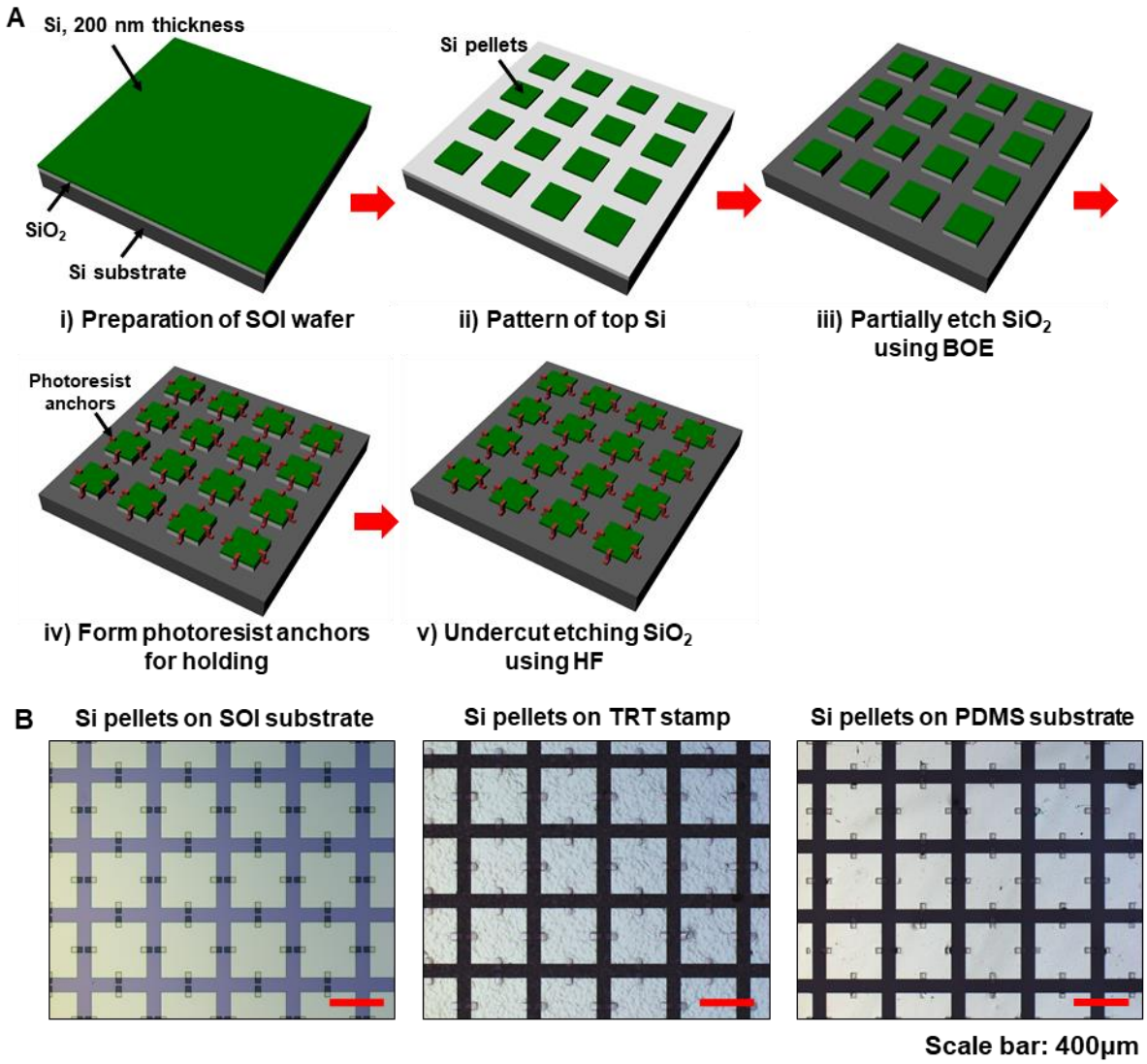

Fig. S2. Fabrication and transfer printing process of ultra-thin Si pellets array. (**A**) Schematic fabrication process and (**B**) optical images of the transfer printing process of ultra-thin Si pellets (200 nm in thickness). Photo Credit: Chengjun Wang, Zhejiang University.

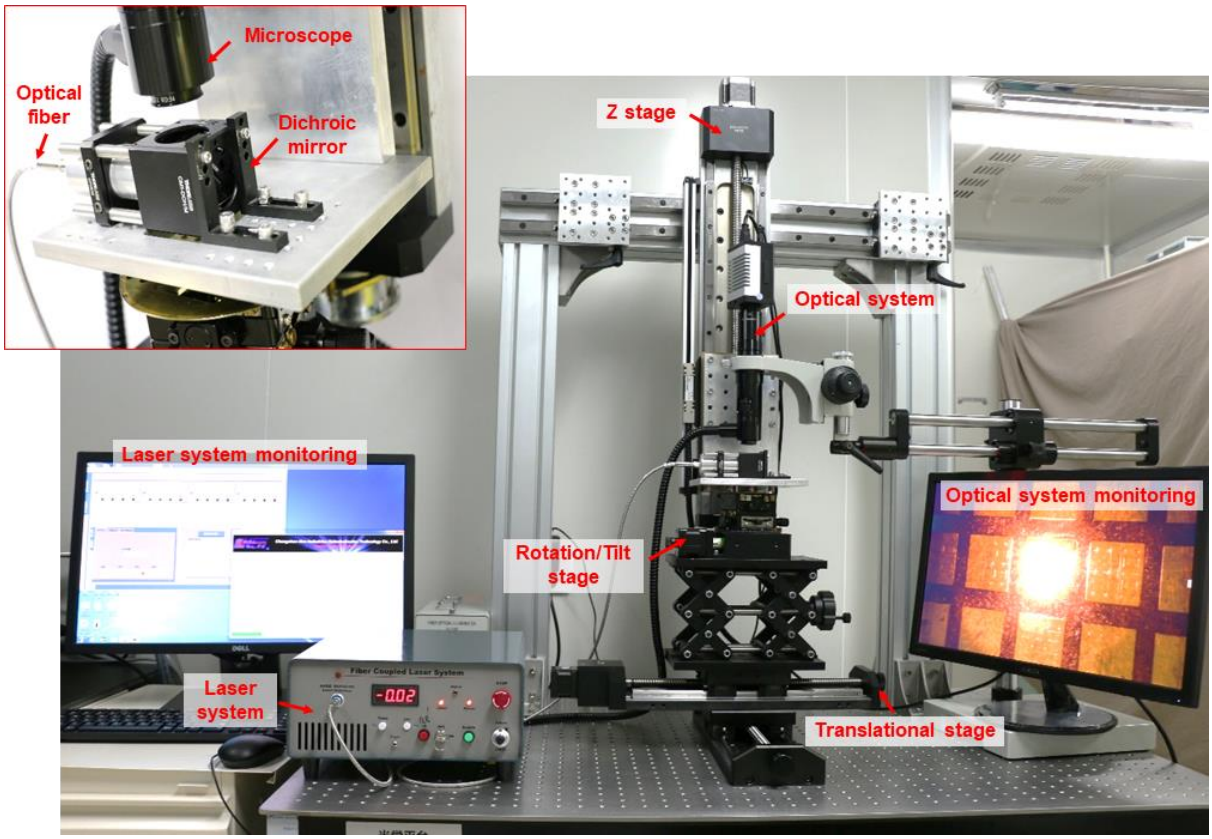

Fig. S3. Photography of the programmable transfer printing system with the automated translational stages. The whole system consists of a laser system, an optical system for in-situ monitoring and the translational stage system for the alignment between the inks and the stamp. The inset illustrates the magnified view of the laser heating head where the laser is guided by an optical fiber into a collimator and focusing lens and then reflected onto the target zone by a dichroic mirror. The dichroic mirror facilitates in-situ monitoring of the heating process. The automated positioning system (Linear stage PSA200, Zolix Inc, China) and the manual triaxial linear stage (EB-050-M-N/F, Everbeing Int'l Corp) are used to control the movement and alignment of the stamp with the laser spot. The placement accuracy for the in-plane movements (the X and Y stages) is 5 μm and 0.9 μm, respectively. Photo Credit: Changhong Linghu, Zhejiang University.

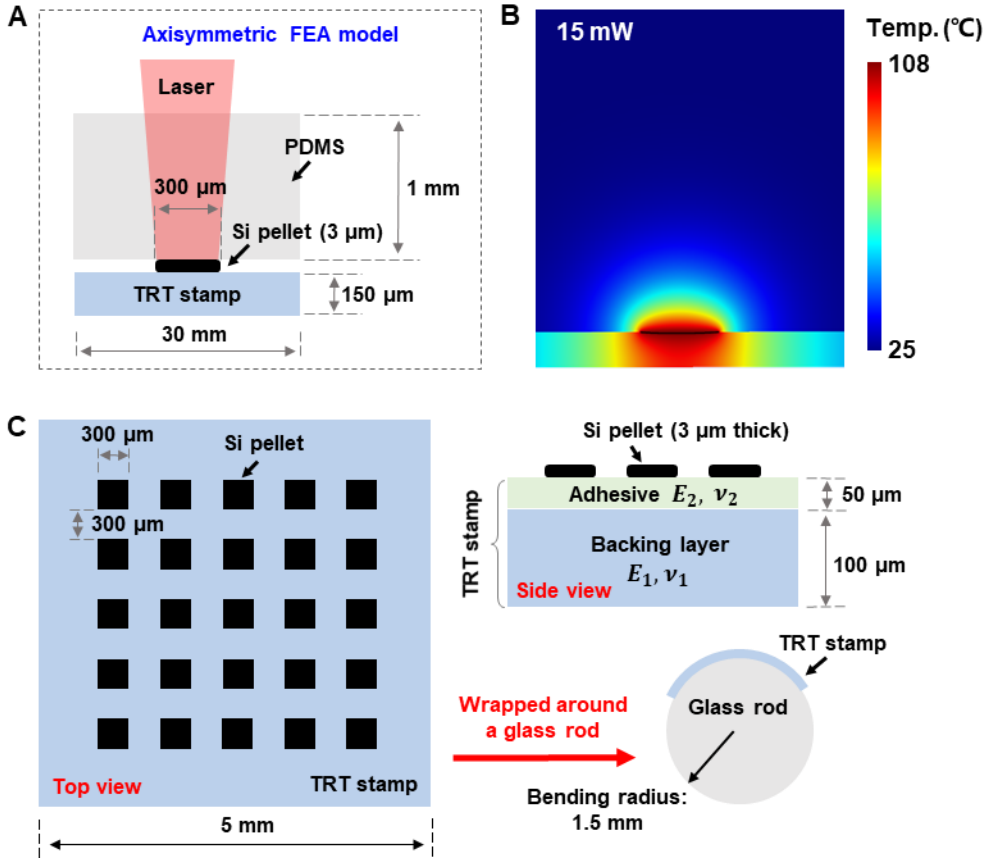

Fig. S4. FEA models and simulated results of Si pellets. (**A**) Cross-sectional image of the axisymmetric FEA model for thermal analysis, where the Si pellet (thickness: 3 μm, diameter: 300 μm) is sandwiched between the TRT stamp and the PDMS receiver substrate. The laser can transmit the PDMS receiver substrate and be absorbed by the Si pellet and therefore heat the TRT stamp around it. (**B**) Simulated temperature increase of the TRT stamp, Si pellet and PDMS receiver substrate at the given laser power of 15 mW. (**C**) Top and side view of Si pellets on the TRT stamp and wrapped around a glass rod to illustrate the FEA geometry model for deformation analysis.

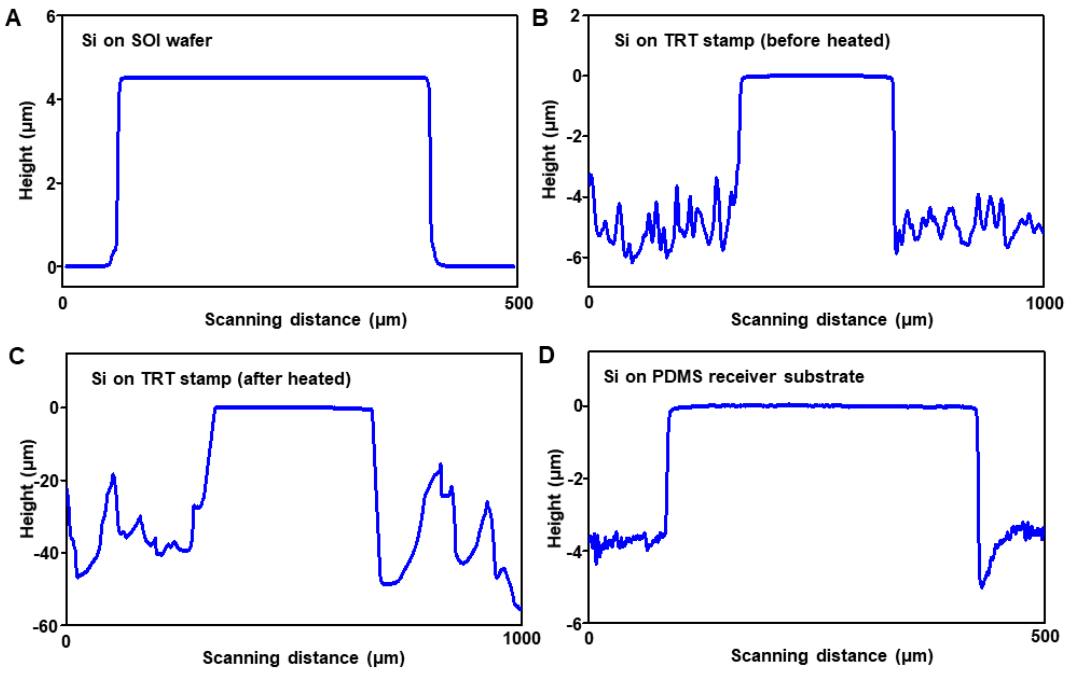

Fig. S5. The measured surface roughness of Si pellet with 3 μm thickness on an SOI wafer, TRT stamp and PDMS receiver substrate respectively.

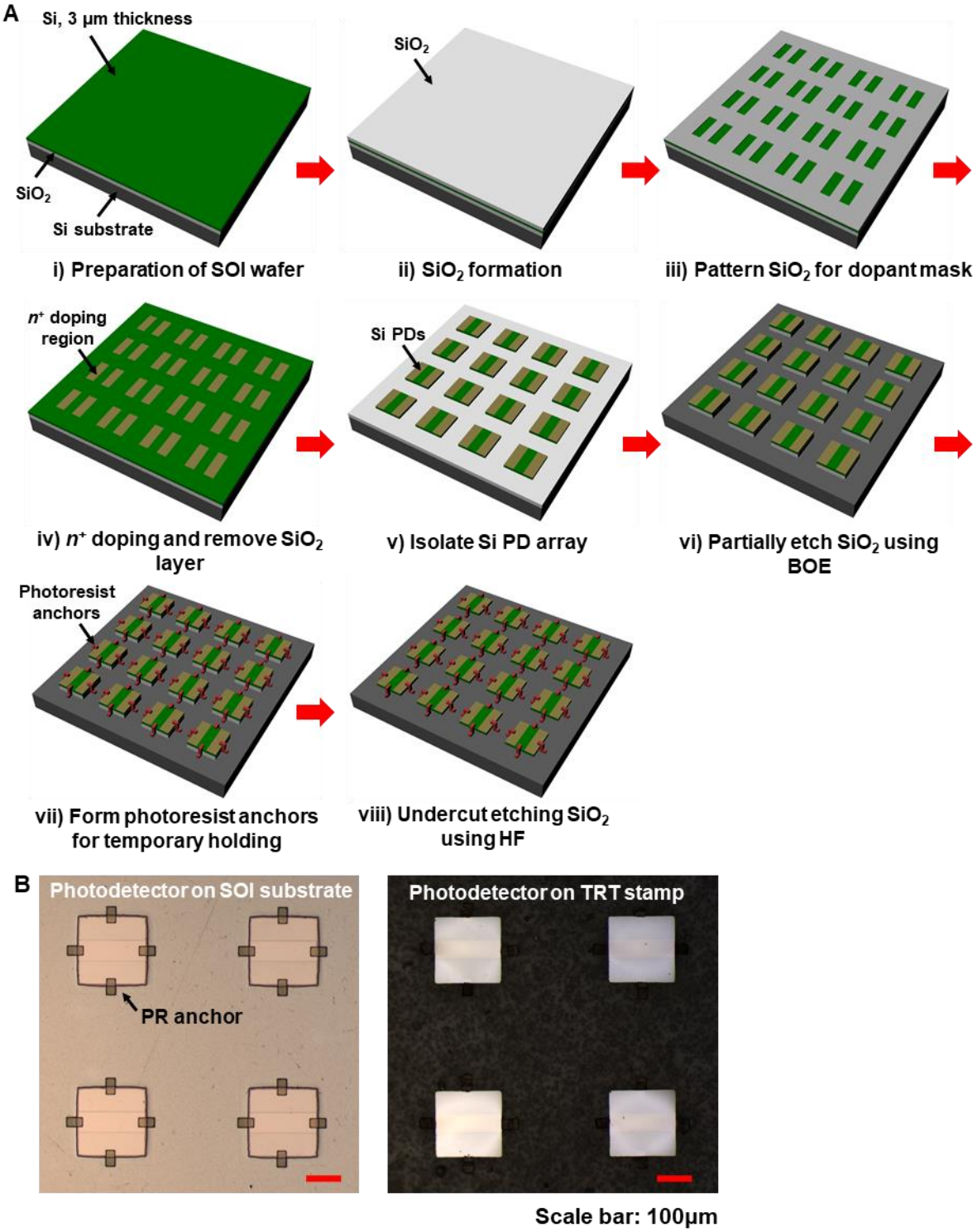

Fig. S6. Fabrication and transfer printing process of ultra-thin Si photodetector array. (**A**) Schematic fabrication process of ultra-thin silicon photodetector array and (**B**) optical images of silicon photodetector array on their fabricated SOI wafer and the TRT stamp, respectively. Photo Credit: Chengjun Wang, Zhejiang University.

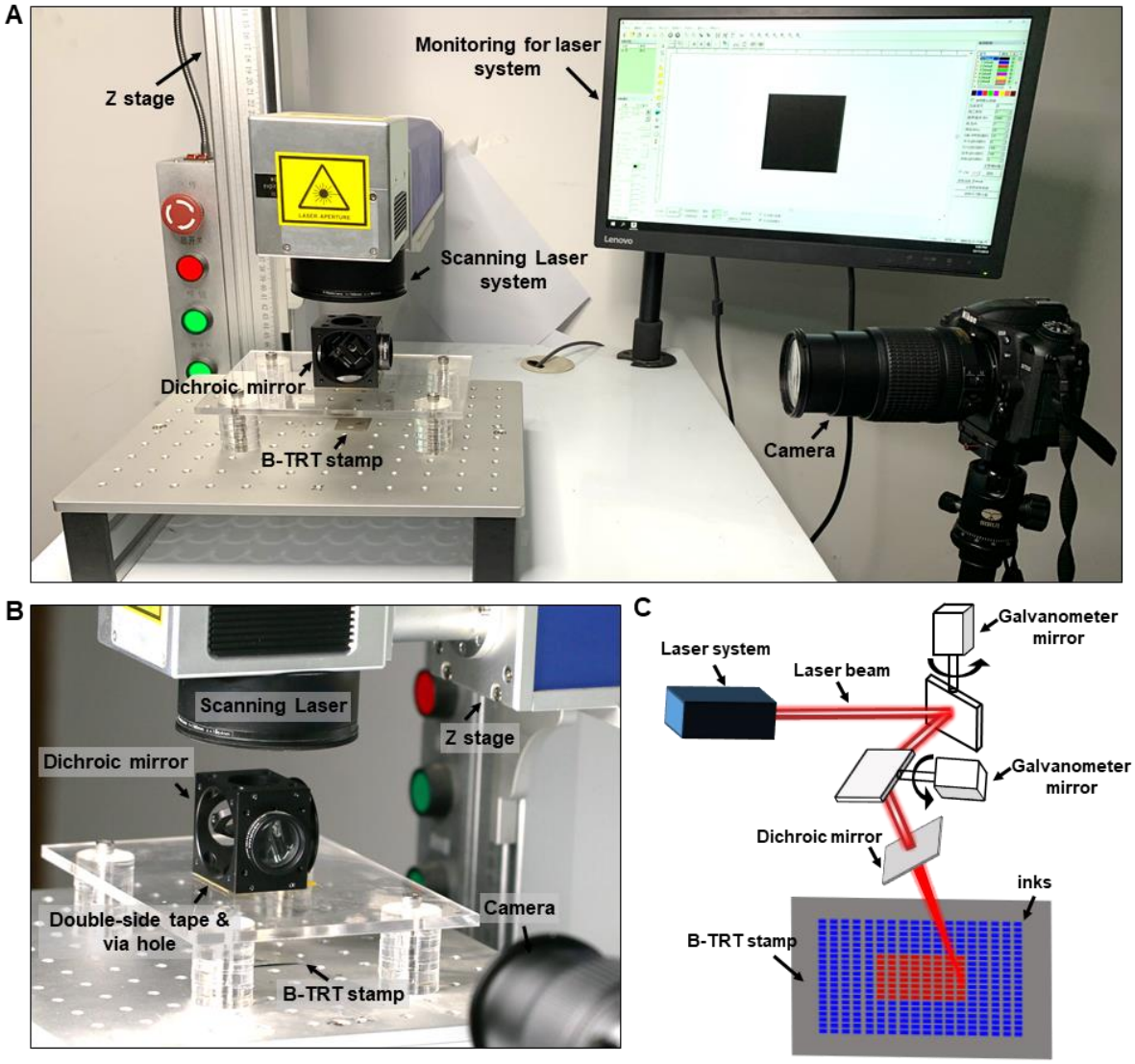

Fig. S7. Programmable transfer printing prototype with scanning laser beam functionality. (**A**) Photography of the programmable transfer printing prototype. The whole system consists of a scanning laser system and a camera for in-situ monitoring. The size of laser spot is around 50 μm in diameter and its in-plane movement accuracy is 10 μm. (**B**) The magnified view of the laser heating head, where a dichroic mirror is employed to facilitate the scanning laser beam and in-situ monitoring simultaneously. (**C**) Schematic image of the galvanometer mirror based scanning laser beam functionality. Photo Credit: Chengjun Wang, Zhejiang University.

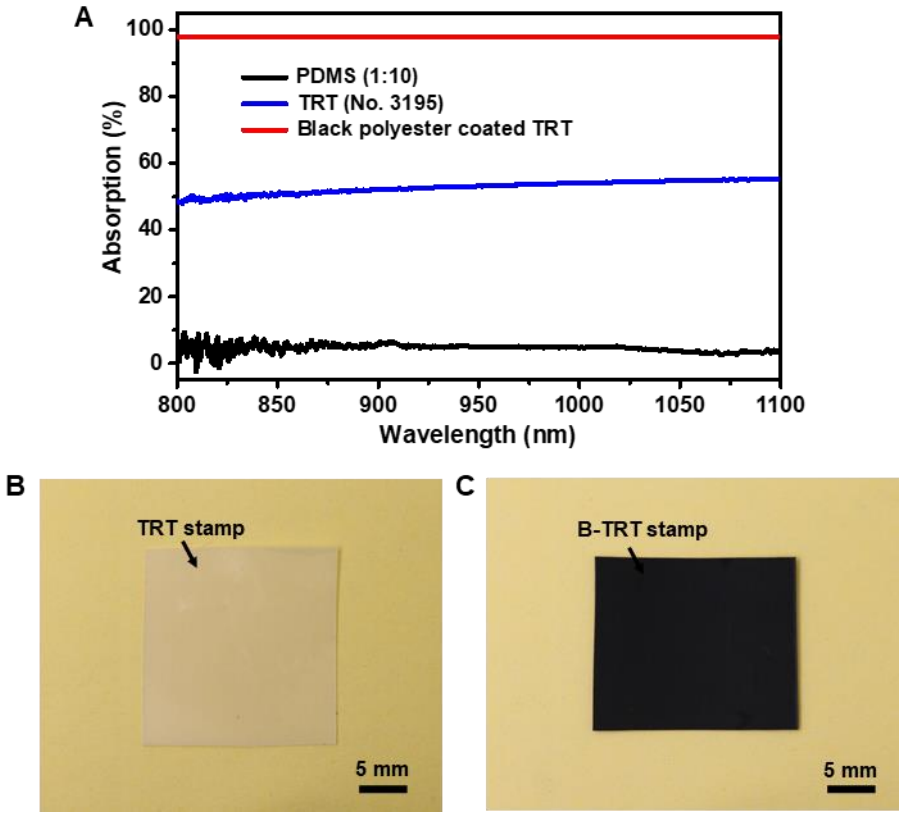

Fig. S8. Optical characteristics of PDMS, TRT and black polyester coated TRT. (**A**) The measured absorption spectrum of the PDMS, TRT and black polyester coated TRT stamp, respectively. Optical images of (**B**) the TRT stamp and (**C**) the B-TRT stamp. Photo Credit: Chengjun Wang, Zhejiang University.

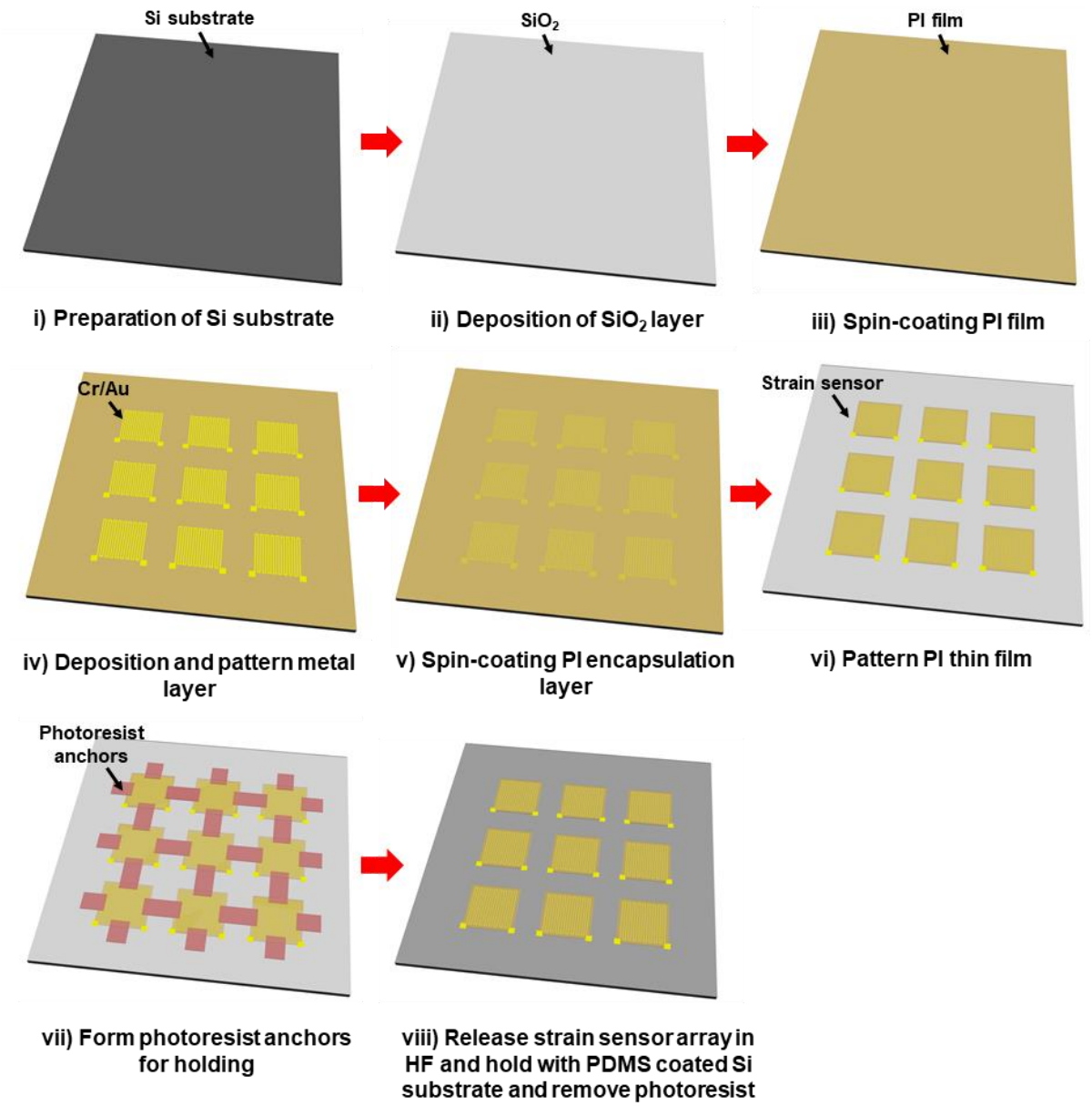

Fig. S9. Schematic fabrication process of the strain sensor array.

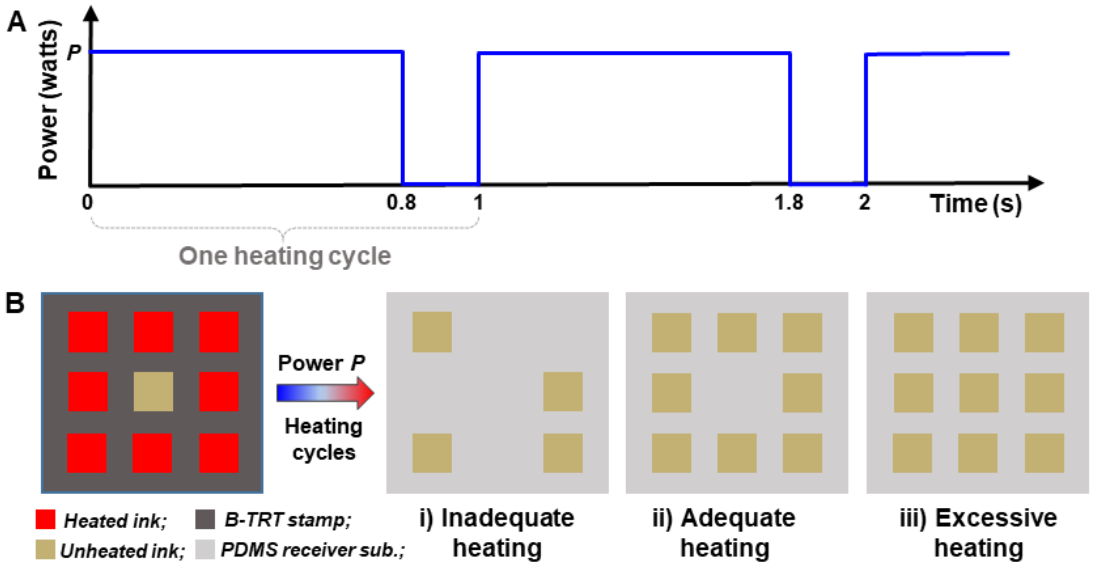

C *Power: 0.15 watts*

Heating cycle	1	2	3	4	5	6	7	8	9
Transfer efficacy	0	5-6	8	8	8	8	8	9	9

Note: *The transfer efficacy represents the quantity of inks successful transferred onto PDMS receiver substrate out of the eight target inks.*

Fig. S10. The transfer efficacy of strain sensor on B-TRT stamp depending on the heating parameters of the localized laser. (**A**) The schematic pulse input of the heating power and duration for one heating cycle of programmable laser system. (**B**) The transfer efficacy of B-TRT stamp under various heating power and duration from a 3×3 array of inks. i) Inadequate heating means that only part of heated inks was successfully transfer-printed on PDMS receiver substrate. ii) Adequate heating means that all inks heated were successfully transfer-printed on PDMS receiver substrate. iii) Excessive heating means that all heated inks and their neighboring inks unheated by the laser were successfully transfer-printed on PDMS receiver substrate. (**C**) The recorded transfer efficacy of B-TRT stamp under various heating cycles. The applied laser power was set as 0.15 watts.

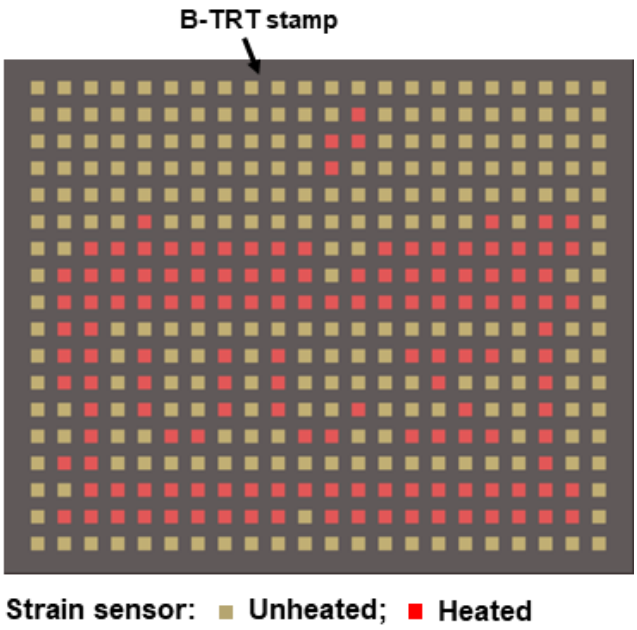

Fig. S11. Schematic image of selective heating pattern of the strain sensors via the automated translational stage.

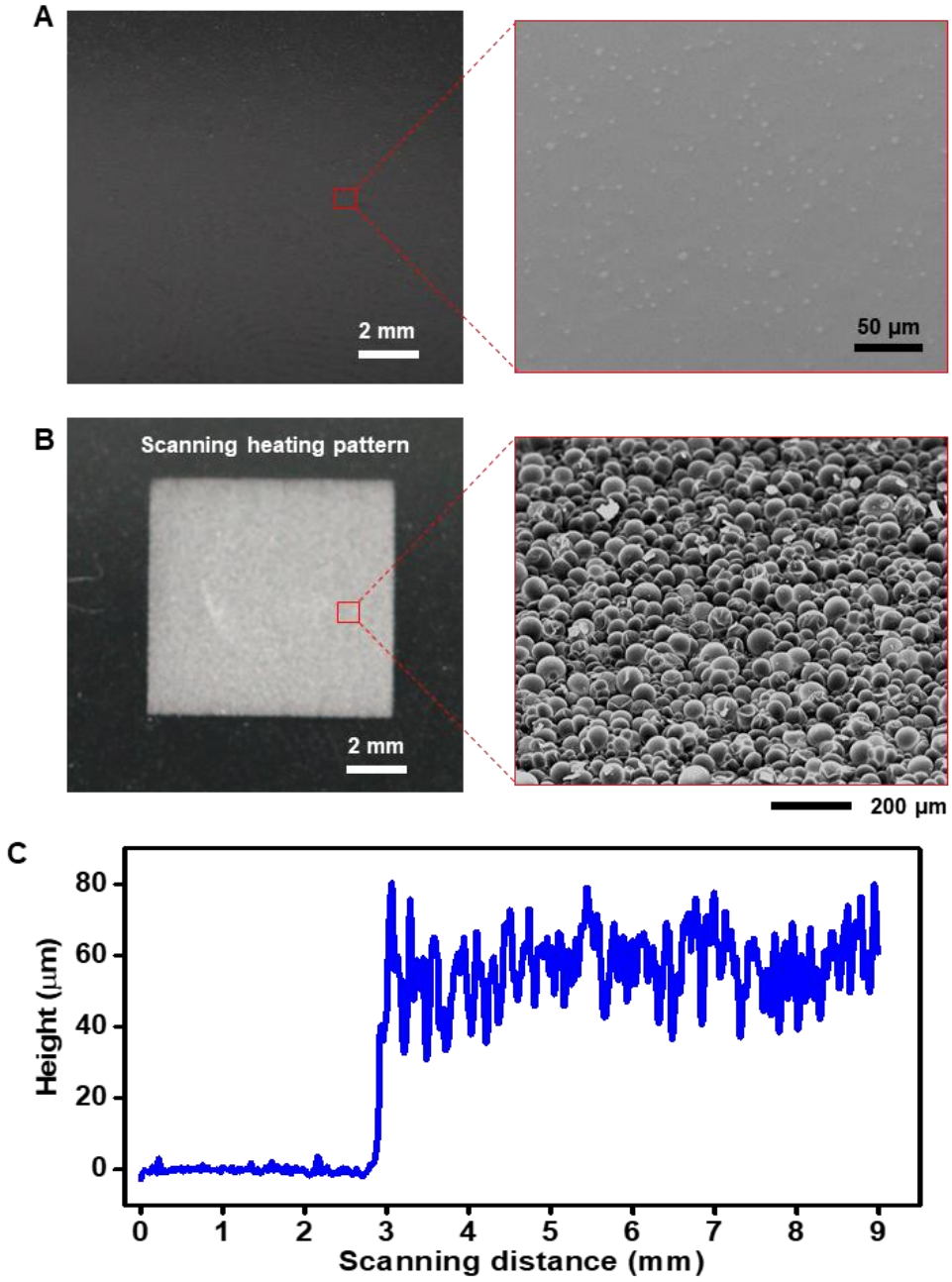

Fig. S12. The scanning heating pattern and measured profile of B-TRT stamp by the scanning laser beam. Optical image of the B-TRT stamp (**A**) before and (**B**) after heated by the scanning laser beam with scanning size of 8 mm×8 mm. (**C**) The measured profile of the B-TRT stamp from unheated region to areas heated by the scanning laser beam. Photo Credit: Chengjun Wang, Zhejiang University.

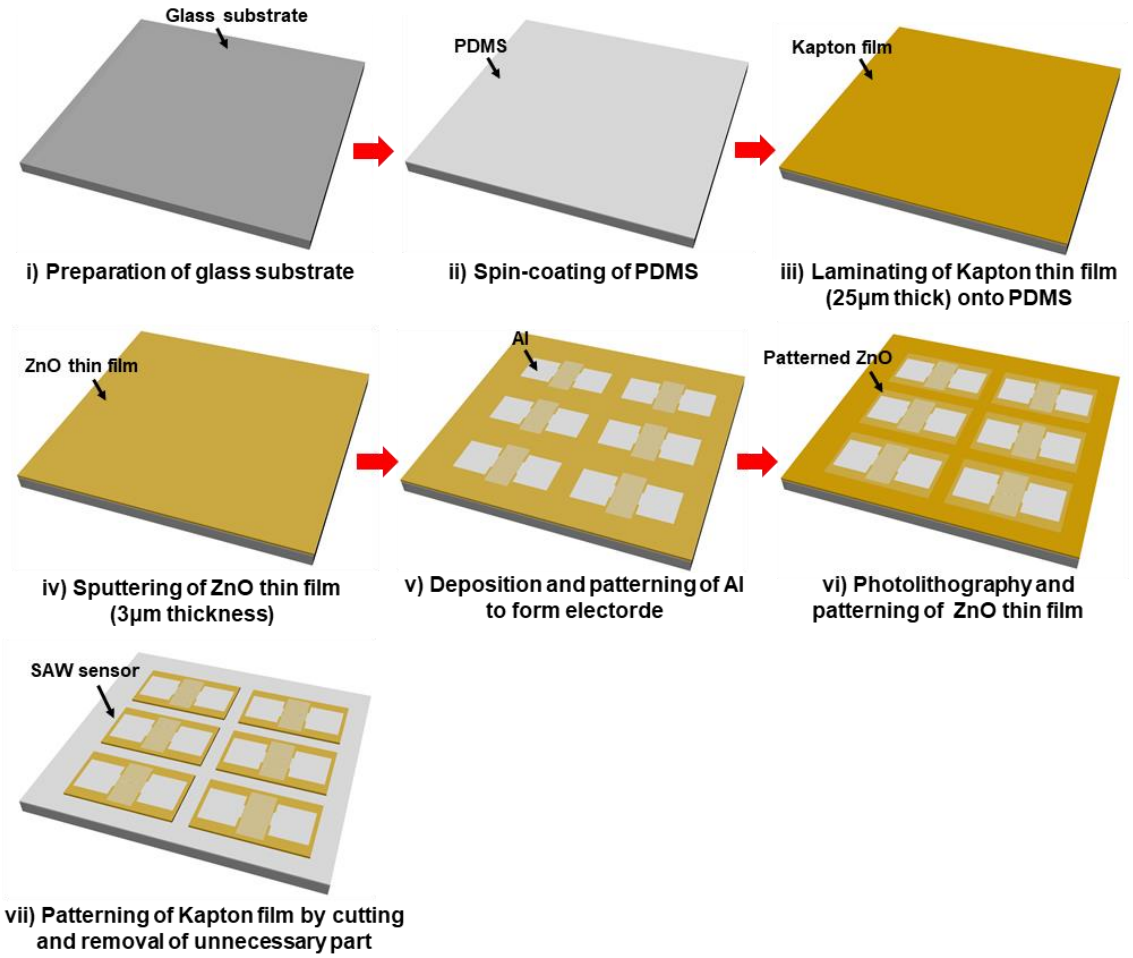

Fig. S13. Schematic fabrication process of the SAW sensor array.

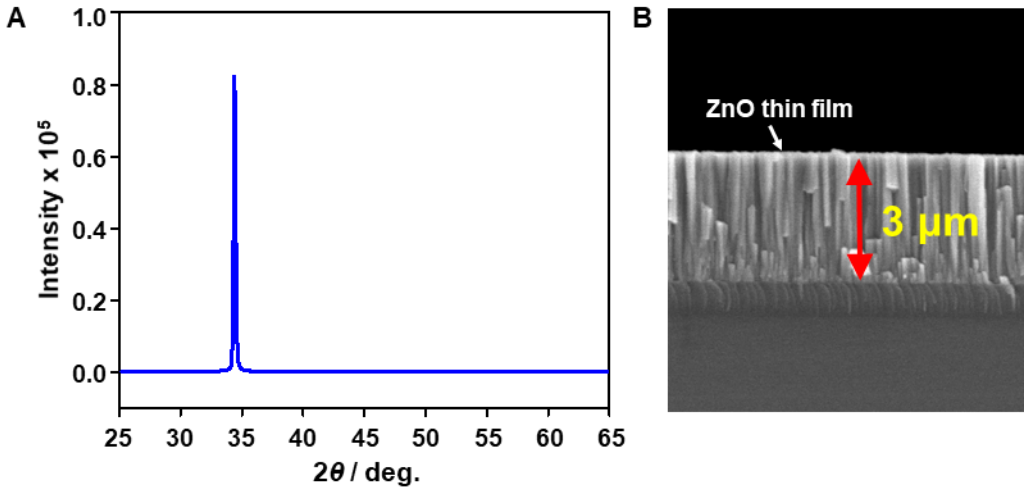

Fig. S14. Characteristics of the ZnO thin film sputtered on the Kapton substrate. (**A**) The measured XRD spectrum of the ZnO thin film at the given temperature, i.e. 70℃. (**B**) SEM image of the cross-section of the ZnO thin film. Photo Credit: Xiang Tao, Zhejiang University.

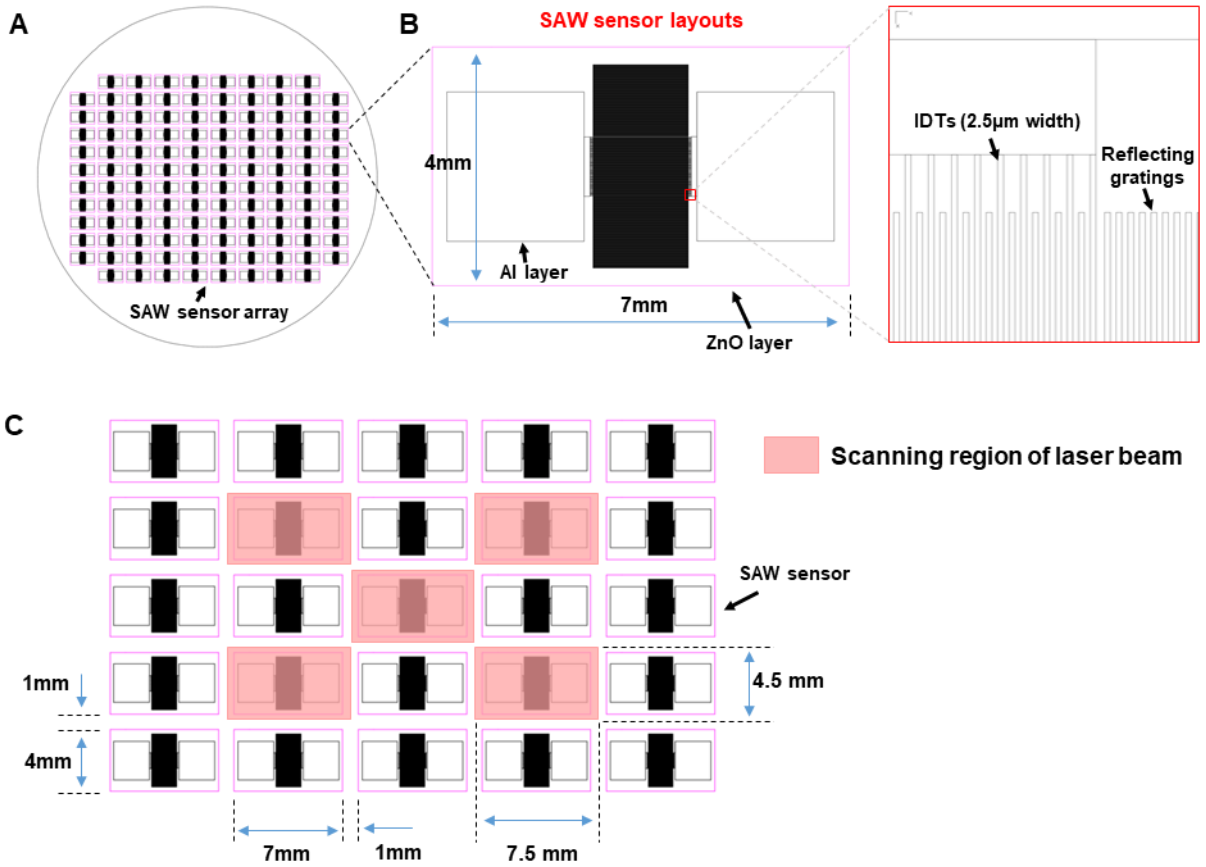

Fig. S15. Layout and selective transfer printing pattern of ZnO based flexible SAW sensor. (**A**) Design of the flexible SAW sensor array on a 4-inch wafer. (**B**) Schematic layout of the SAW sensor with the magnified view at its right-hand side. (**C**) The programmable and scalable heating pattern of SAW sensors via the scanning laser beam functionality.

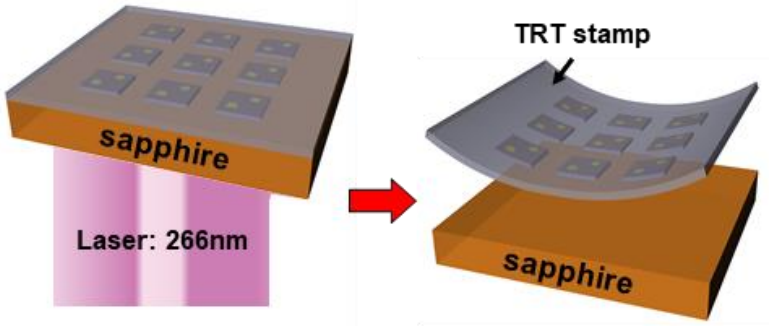

Fig. S16. Schematic illustration of the InGaN μ-LEDs transferred from their fabricated sapphire wafer to TRT stamp by the standard laser lift-off process.

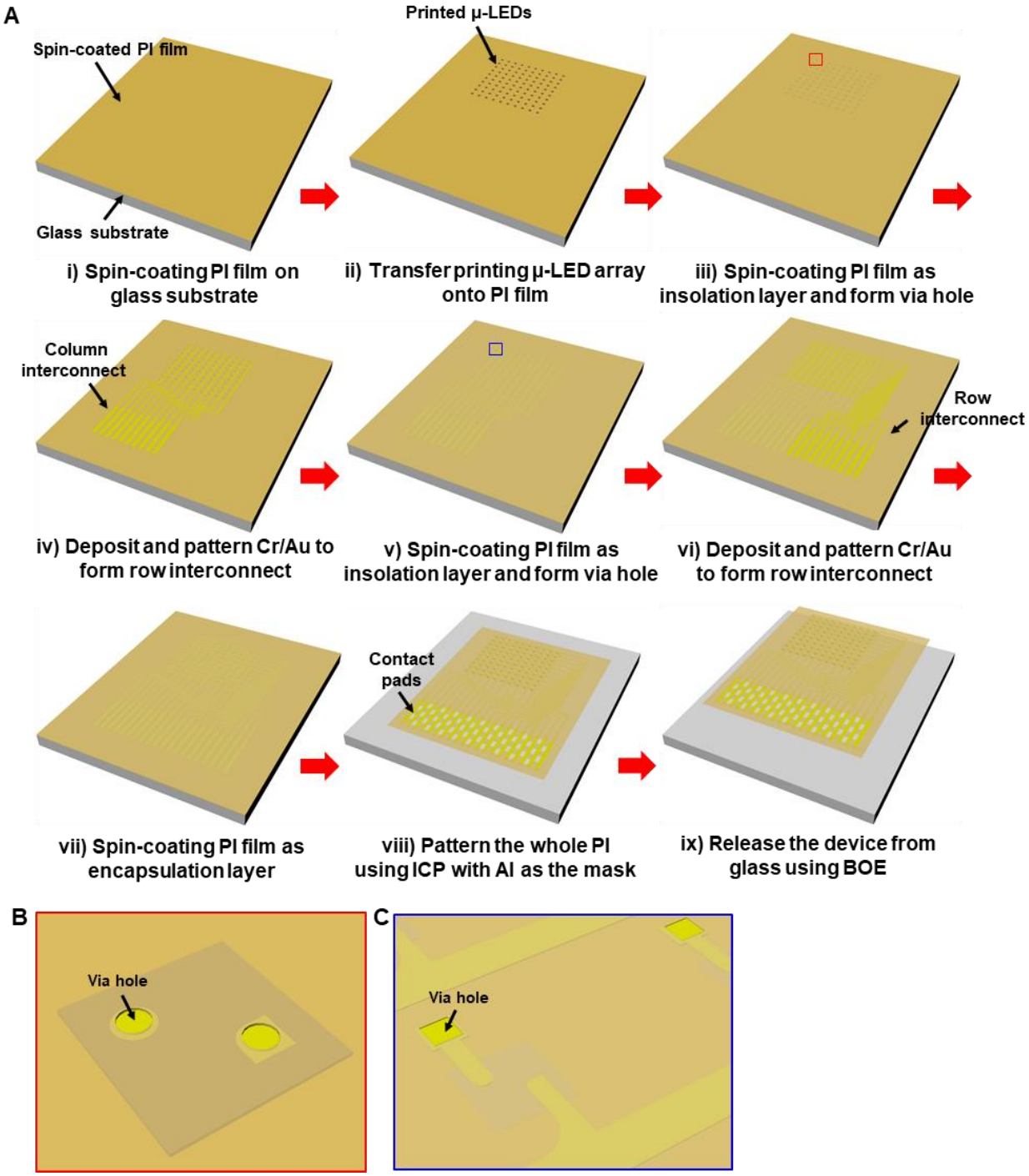

Fig. S17. Fabrication process of the μ-LED array based flexible display. (**A**) Schematic fabrication process of the μ-LED array based flexible display with (**B**)-(**C**) the magnified view marked in (**A**)-iii) and v).

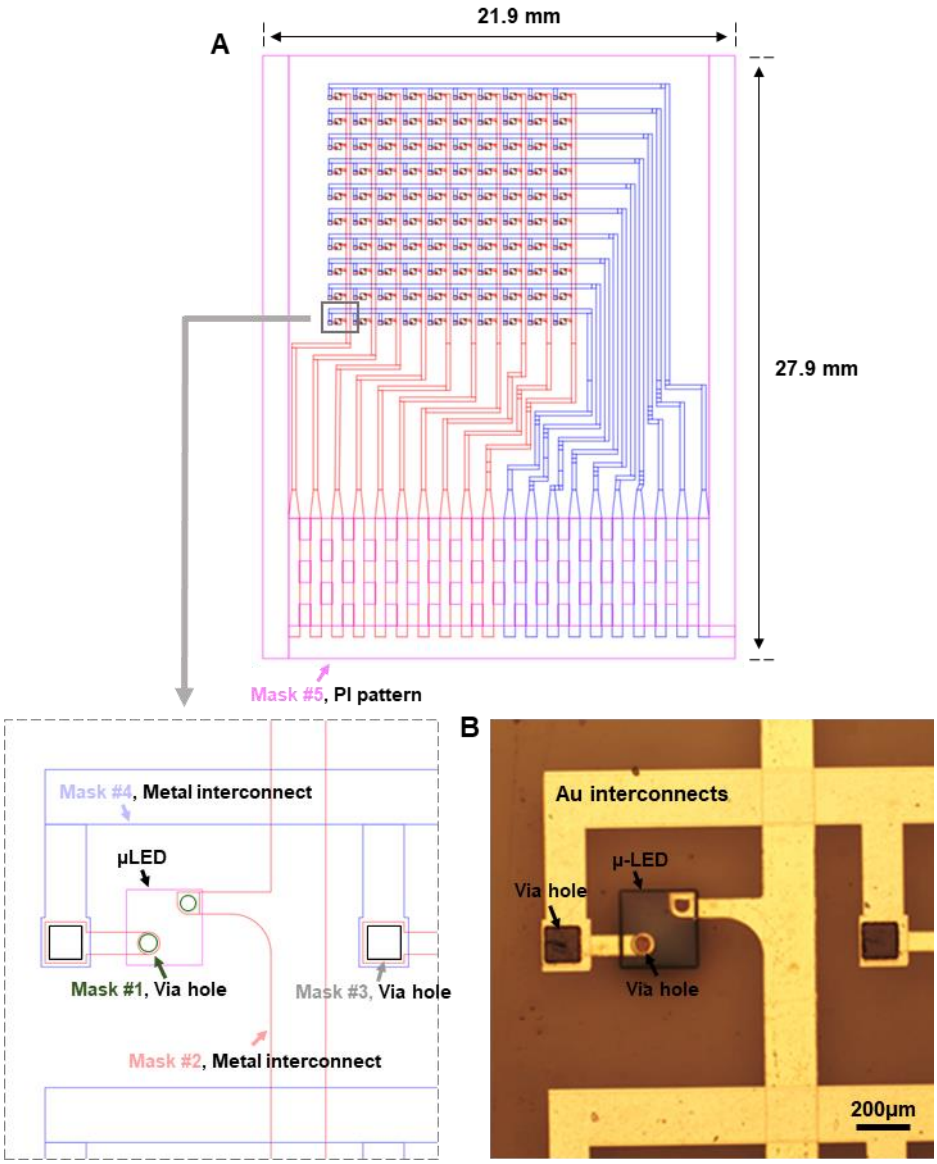

Fig. S18. Layout of ultra-thin μ-LED array based flexible display. (**A**) Design of ultra-thin μ-LED array based flexible display. (**B**) Optical image of the μ-LED connected with row and column interconnect through via holes. Photo Credit: Chengjun Wang, Zhejiang University.

Legends for movies S1 to S2.

Movie S1. Programmable and scalable printing of strain sensors on the B-TRT stamp to PDMS substrate via the scanning laser beam.

Movie S2. Flexible inorganic μ-LED display.